Available online at www.sciencedirect.com
SCIENCE DIRECT®

Journal of the European Ceramic Society 24 (2004) 1251–1257
www.elsevier.com/locate/jeurceramsoc

Transport in electroceramics: micro- and nano-structural aspects

Joachim Maier*

Max-Planck-Institut für Festkörperforschung, Heisenbergstraße 1, 70569 Stuttgart, Germany

Abstract

Point defects are of paramount importance for electroceramics. They are key structure elements as regards materials functionality; but, in addition, they are also decisive for chemical kinetics, hence for preparation, conditioning, annealing and degradation phenomena. Concentrations and mobilities of these charge carriers are significantly changed at or near interfaces (or more generally higher dimensional defects) giving rise to depletion, accumulation, and inversion layers with respect to ionic and electronic carriers and hence to distinct electrical and chemical effects. It is discussed how these effects can be explained and how such knowledge can be used to design electroceramics purposefully. Examples refer to ionically or mixed conducting oxides and halides. Finally, in nano-structured materials the spacing of interfaces becomes relevant in that local properties can be severely affected. Such size effects do not only lead to confinement effects in the case of electronic carriers but also to anomalies with respect to ion conduction and mass transport. The potential of the nano-regime for electrical and chemical properties of electroceramics is discussed in the framework of a ''soft materials science''.

Keywords: Defects; Functional applications; Interfaces; Ionic conductivity; Nano-ionics

1. Introduction

Defects are of paramount significance for electroceramics. While the number of defects increases with dimensionality, their mobility decreases. As a consequence, point defects are even present under equilibrium conditions and in fact are often in local equilibrium under operational conditions, whilst interfaces as two-dimensional defects are typical frozen-in structure elements, introduced and shaped by the preparation. Nonetheless, and this will be largely the scope of this paper, they set important boundary conditions for the point defect concentrations. One-dimensional defects such as (isolated) dislocations play an intermediate role, they are also typical non-equilibrium phenomena but often mobile enough to be healed out at operation temperatures. If we distribute N_D zero-, one- or two-dimensional defects (dimensionality D) randomly within a cubic crystal containing N uncharged atoms of the same kind, the equilibrium concentration (arc denotes equilibrium value) is (see Refs. 1 and 2)

$$\widehat{N}_D \sim N^{1-D/3}\exp -\frac{\Delta G_D^*}{kT}. \quad (1)$$

The reduction of $\widehat{N}_D$ with increasing D is due to the decreased number of available states $N^{1-D/3}$ but more importantly due to the increased free formation enthalpy per defect. As a consequence, realistic numbers for ΔG_D* lead to an equilibrium number of defects, much less than unity (i.e. virtually zero) if $D=2$ or 3. This is even more so if the crystal size (i.e. N) is small. Owing to a perceptible mobility of dislocations, it is often assumed that free dislocations are absent in nanocrystalline matter. Hence in this paper we ignore dislocations, while we consider interfaces as metastable frozen-in structure elements. Point defects are considered to be in local equilibrium (usually in one sublattice) or (as dopant defects or defects in other sublattices) totally frozen.

The role of point defects in solids as decisive mobile atomic/ionic excitations and hence as charge carriers is analogous to that of H_3O^+ (excess proton) and OH^- (lacking proton) in water, which highlights the significance not only for the electrical transport but also for mass transport and chemical kinetics.

Point defects—in a wider sense, also including the electronic carriers (excess electron, and lacking electron = electron hole)—play a direct prime role for the function of many electroceramics, as typically used in electrochemical devices such as batteries, fuel cells,

* Tel.: +49-711-689-1720; fax: +49-711-689-1722.
E-mail address: s.weiglein@fkf.mpg.de (J. Maier).

0955-2219/$ - see front matter © 2003 Elsevier Ltd. All rights reserved.
doi:10.1016/S0955-2219(03)00507-7

ceramic membranes, electrochemical sensors and electrochromic windows. In addition to that—as they are indispensable for the chemical kinetics—they play a decisive role in preparation, processing, conditioning and degradation of electroceramics even if they are not very relevant for the function.

Consequently, it is of high priority to know the control parameters for tailoring the defect chemistry in a given electroceramic material. This will be briefly discussed.

2. Parameters controlling point defect chemistry

Let us first consider the bulk of a binary MX under equilibrium conditions. Under Brouwer conditions (only two majority carriers), the solution for the defect concentration (c_j) reads

$$\widehat{c_j} = \alpha_j P_{X_2}^{N_j} C^{M_j} \prod_{\mathrm{r}} K_{\mathrm{r}}^{\gamma_{\mathrm{r}j}}(T), \tag{2}$$

revealing the control parameters, component potential (P_{X_2}), doping content (C) and temperature (α being a constant). Note that the boundaries of the windows in which Eq. (2) holds—and hence the characteristic exponents (being rational numbers) N_j; M_j; $\gamma_{\mathrm{r}j}$—depend unambiguously on P, C, T (we consider the hydrostatic pressure to be fixed and ignore outer fields). Since also the signs of the characteristic exponents depend on the nature of the defects usually in a predictable way, the following qualitative rules can be set up:

1. *Component activity rule (P-rule)*. If we increase the partial pressure of the electronegative (positive) component, we increase (decrease) the number of holes and decrease (increase) the number of excess electrons; we increase (decrease) the numbers of all defects which individually increase (decrease) the X–M stoichiometry and decrease (increase) the others. As the other rules, these statements—since compensation effects do not occur (see Ref.2)—are not trivial in that they would simply follow from conservation laws, but reflect also the individual mass actions.
2. *Rule of (homogeneous) doping (C-rule)*. If the effective charge of the dopant defect is positive (negative), we increase (decrease) the concentration of all negatively charged defects and decrease (increase) the concentration of all positively charged defects. Again compensation effects (that would be allowed within the electroneutrality equation) do not occur.
3. *Temperature rule (T-rule)*. Temperature increase (decrease) favours endothermic (exothermic) reactions. Since the total T-dependence is determined by a combination of formation energies, the final result is not always obvious. However, usually, the defect concentrations rise with increasing temperature.

In more complex situations and multinary systems Eq. (2) has to be extended as

$$\widehat{c_j} = \alpha_j \left(\prod_n P_n^{N_{nj}} \right) C^{M_j} \left(\prod_{\mathrm{r}} K_{\mathrm{r}}^{\gamma_{\mathrm{r}j}}(T) \right). \tag{3}$$

As in Eq. (2) we have to distinguish between in situ parameters that can be reversibly changed ($\prod_n P_n^{N_{nj}}$) and ex situ parameters (C^{M_j}) the change of which requires new preparation (or at least a temperature treatment).[2] A typical ex situ parameter is the doping content but also native defects that are frozen under operational conditions. If a high enough temperature is chosen, their incorporation becomes reversible, they disappear from the list of ex situ parameters, instead, new equilibria (segregation equilibria involving "dopants"; defect equilibria involving the "low-mobile" defects) become relevant modifying the ($\prod_{\mathrm{r}} K_{\mathrm{r}}^{\gamma_{\mathrm{r}j}}(T)$)-Term but in the case of segregation equilibria also introducing new in situ parameters. A related second example concerns the water-containing proton conducting oxides, e.g., $BaCeO_3$ (H_2O, Y_2O_3). Whilst the C-term contains the Y-concentration but also immobilised Ba- and Ca-defects, the P-list now contains in addition to P_{O_2} also P_{H_2O} (or P_{H_2}). At lower temperature the interaction of H_2O with the oxide may freeze, P_{H_2O} disappears from the P-list, and [H_2O], or more specifically [$OH_O^{\bullet}$], appears in the C-term; a similar transition occurs with respect to P_{O_2} and [$V_O^{\bullet\bullet}$] at reduced temperatures.[3–6]

3. Interfacial effects on defect chemistry and transport

It has been shown in detail that internal boundaries also lead to severe changes in the defect chemistry via space charge effects (cf. role of heterogeneous doping).[7] In that sense they are also ex situ parameters. However, now the calculation cannot resort on electroneutrality. In addition, the structurally modified part of the interface (compared to the bulk)—the interfacial core—will exhibit its own defect chemistry and special mobilities, and can hence, provide fast pathways or obstacles (in addition to space charge effects).

Fig. 1 gives the most simple example of an elementary crystal and the formation of a vacancy therein. Whilst for the formation of a bulk vacancy three bonds (six neighbours assumed) have to be broken, only two have to be broken if a vacancy is formed in the surface. If we ignore relaxation effects this corresponds to a factor of 2/3 as far as the standard chemical potential is assumed. Similarly the bond strength in a given interfacial region is different (by a factor B) and we hence expect a different

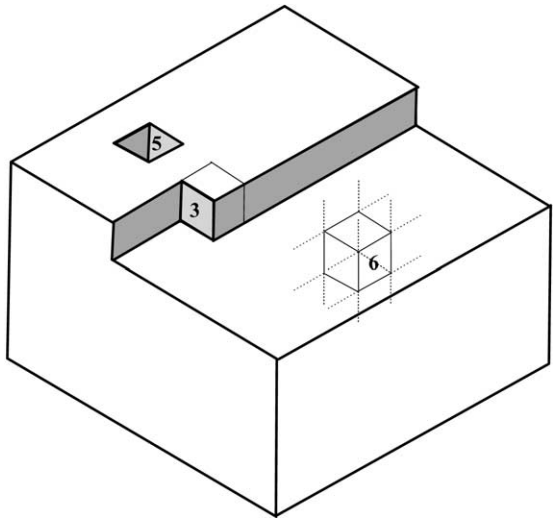

Fig. 1. The transfer of an elementary cube from the interior to the surface (kink corner) is accompanied by a loss of three bonds, while the transfer of a cube from the surface to the same site is accompanied by two bonds. The labels 6, 5, 3 indicate the number of bonds of the bulk particle, the surface particle and the kink particle in the perfect solid, respectively.[8]

(presumably lower) standard chemical potential. If we treat the core of the interface as an electroneutral region, this factor B enters exponentially [see e.g., Eqs. (1)–(3)] leading to severely changed defect concentrations. In ionic crystals the situation is more complicated: not only can the valencies of defects be different if we compare bulk and interfaces, the contact of two regions of different standard potentials (bulk and interfacial core) necessarily leads to a charging modifying the core defect concentration and leading to space charge effects in the crystal parts adjacent to the core. Approximately we encounter the following situation: The interface is structurally different from the bulk and charged, it exhibits carrier concentrations and mobilities different from the bulk. On both sides space charge regions join (extension determined by Debye-length, λ, proportional to the reciprocal square root of bulk majority concentration) with severely modified concentrations of carriers exhibiting bulk mobilities to a first approximation. Regarding the question whether core or space charges are more mobile, the following rule of thumb may be stated: In high mobility materials usually the bulk structure is optimised for point defect motion (e.g., silver halides), then a structural modification as occuring in the grain boundary is likely to depress the mobility. The inverse is true for materials with very low defect mobilities in the bulk (e.g., Al_2O_3, or metals at lower temperatures); there any structural perturbation is likely to increase the mobility significantly.

In the space charge regions, the defect concentration decays from the boundary value to the bulk value c_∞ via Gouy–Chapman, Mott–Schottky or more complicated types of profiles. Supposing the bulk defect chemistry and hence c_∞ to be known, the remaining task is to get access to c_0 (or the space charge potential $\phi_0-\phi_\infty$); c_0 can be referred to the core charge the knowledge of which requires the knowledge of core defect chemistry. Such an establishing of core models is a major challenge of interfacial solid state science. An appropriate phenomenological framework is given by the core-space charge model[9,10] and a more detailed treatment is provided by Ref. 2.

In the space charge zones, the defect profiles (charge number z_j) are determined by

$$c_j^{1/z_j}(x) = \exp -\frac{F\Delta\phi(x)}{\mathrm{RT}}. \tag{4}$$

By analogy to the rule of homogeneous doping which we can qualitatively formulate as

$$\frac{z_j\delta c_j}{z\delta C} < 0, \tag{5}$$

we can state the rule of heterogeneous doping, viz.

$$\frac{z_j\delta c_j}{\delta\Sigma} < 0, \tag{6}$$

where Σ is the surface charge density. Eq. (6) can be reformulated as follows:

4. Rule of heterogeneous doping: Is the interfacial core charge positive (negative), then the concentrations of all negative defects are increased in the space charge region [$\Delta\phi$ in Eq. (4) is then negative] whilst the concentrations of all positive (negative) defects are decreased (suffcient mobilities presupposed).

The local effects and sometimes also the overall effects can be much higher than in the case of homogeneous doping. The fact that the boundary effects are locally restricted and inhomogeneous, leads to non-trivial superposition patterns of boundary and bulk effects as well as to anisotropy phenomena. The most simple approach which represents a reasonable first approximation is the bricklayer model (see Fig. 2). Superimposing bulk, core and space charge effects according to Fig. 2 leads (for a single carrier situation) to:[12]

$$\hat{\sigma}_\mathrm{m} = \frac{\hat{\sigma}_\infty\hat{\sigma}_\mathrm{L}^\perp + \beta_\mathrm{L}^\parallel\varphi_\mathrm{L}\hat{\sigma}_\mathrm{L}^\parallel\sigma_\mathrm{L}^\perp}{\hat{\sigma}_\mathrm{L}^\perp + \beta_\mathrm{L}^\perp\varphi_\mathrm{L}\hat{\sigma}_\infty}, \tag{7}$$

where $\hat{\sigma}_\mathrm{L}^\parallel$ and $\sigma_\mathrm{L}^\perp$ are the contributions of parallel and perpendicular layers to the complex conductivity being differently composed of core and space charge contributions,[12] φ_L is the proportion of interfaces (by volume) and β measures the fraction that contributes to the path.

A special role is played by the surfaces where the gas–solid interactions take place with sometimes complicated mechanisms and reaction schemes. For a more detailed treatment of this the reader is referred to Ref. 13, here we will focus on solid–solid boundaries.

4. Examples of accumulation and depletion layers

A striking example for the efficacy of heterogeneous doping is the admixture of insulating but surface active second phase particles, e.g., Al_2O_3 to AgCl, the positive surface charge due to Ag^+ adsorption is equivalent to a drastic increase of silver vacancies in the adjacent boundary regions.[7] At the contact of two ionic conductors (apart from phase equilibration) a redistribution of ions over both space charge regions [and of course also of electrons, see Eq. (4)], occurs; this explains drastic conductivity anomalies in two phase systems. (An example of space charge effects at the gas–solid interface is the NH_3/AgCl contact which leads to the possibility of sensing acid-base active gases by a Taguchi-analogue.)[14]

In AgCl-polycrystals space charge effects have also been locally observed (see Fig. 3).

Both effects can be enhanced by introducing chemicals into the grain boundaries that are ionically attractive such as NH_3 for Ag^+ or SbF_5 for F^-.[7,17]

Severe depletion effects are observed in acceptor doped oxides (Fe-doped $SrTiO_3$, Y-doped ZrO_2 or CeO_2). There a positive space charge potential occurs according to Refs. 5,18–23. As a consequence, holes and oxygen vacancies are depleted. The decreased hole concentration leads to perceptible grain boundary resistances (as regards the electronic conductivity, see Fig. 4). By separating electronic and ionic conductivities in single and bi-crystals it could be shown that also the ionic conductivity is decreased, in fact decreased much more severely in accordance with Eq. (4) ($z=2$).[18] The simultaneous decrease of $h^\bullet$ and $V_O^{\bullet\bullet}$ leads also to a pronounced chemical resistance with respect to oxygen incorporation. This is because at high oxygen partial pressures the presence and mobility of both carriers is important for an effectively neutral mass transport. In Fe-doped $SrTiO_3$ the transport is indicated by colour jumps over the boundaries.[22] All these aspects can be consistently described in $SrTiO_3$.

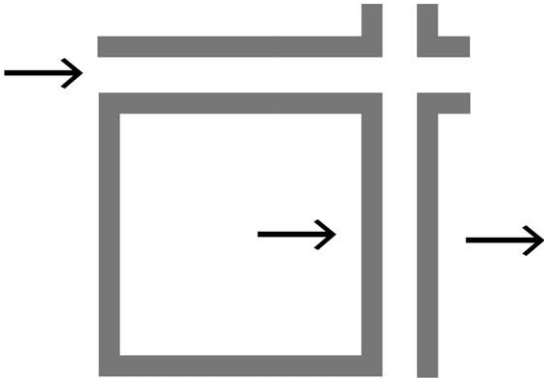

Fig. 2. The contribution of the different pathways to the electric transport from the left to the right in a polycrystalline bricklayer sample.[11]

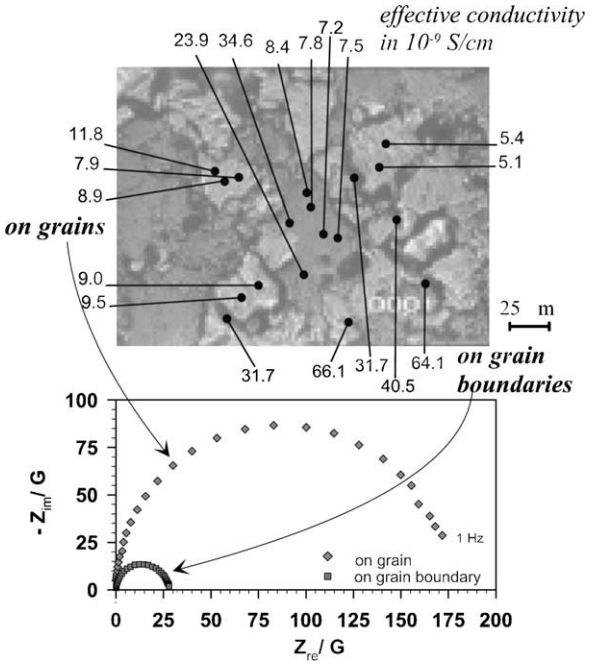

Fig. 3. Local measurement of enhanced grain boundary conductivities (AgCl). Top: microstructure and contact topology; bottom: impedance spectra.[15]

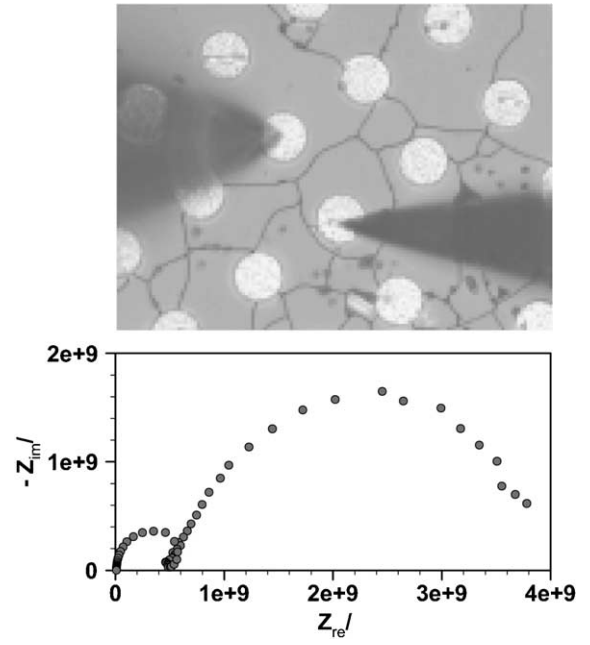

Fig. 4. Local measurement of depressed grain boundary conductivities ($SrTiO_3$). Top: microstructure and contact topology, bottom: impedance spectrum.[16]

There are (apart from blocking effects by impurity phases) many indications of depletion effects also at YSZ boundaries.[24] Nominally the Debye-length (according to high Y-content) is so small that only a rigid double layer (or more precisely triple layer) should be expected. The fact that a Mott–Schottky layer may be realised rather than a Gouy–Chapman layer leads to a formal increase of the space charge width. The same holds true if the interactions between Y'_{Zr} and oxygen vacancies are taken account of. Yet, this effect on λ is not so pronounced. Nevertheless, the non-ideality of YSZ may provide a more realistic argument that might explain that experimentally larger effective widths are measured: severe defect concentrations should imply a tendency to structural rearrangements tending to make the defects locally more regular structural units and to immobilise them.

A further interesting feature of the above space charge situation (positive space charge potential) is the increase in the e′-concentration. In situations in which [e′] is already quite high in the bulk, this may lead to n-type conductivity in the boundary regions.[25] This point will prove significant in the next section.

5. Nano-structured materials: the spacing of interfaces as control parameter

Nano-structured materials necessarily possess a high proportion of interfaces (φ_{bg}),typically more than 10% of the atoms sit in what can be called interfacial core. Hence we expect pronounced size effects. In this context it proves worthwhile (even though a clear distinction is not always feasible) to distinguish between "trivial size effects" whereby the same effects as described above, are realised but appear in an augmented way owing to the increased φ_{bg}, and "true" size effects whereby also local properties are changed (depends on the interfacial spacing too).[8,11,13,26]

Such true size effects can be primarily due to space charge overlap ($L \leqslant 4\lambda$) or due to structural changes ($L \leqslant 2\ \ell$) unlike λ (ℓ is an ad-hoc size parameter above which the abrupt structural model applies). If we ignore materials and microstructural situations characterised by elastic (i.e. also structural) effects of long-range and concentrate on situations with dilute defect chemistry (i.e. $\ell \ll \lambda$), we should be able to observe both phenomena separately. Indeed in many materials $\lambda \sim 10$ nm while $\ell \sim 1$ nm.[13] The first effect affects the electrical potential, the second the standard chemical potential. A minimum ℓ-value should be given by the size of the relaxation sphere around a defect. This is similar in the case of small polarons, while for wide bands the standard chemical potentials of electronic carriers may be shifted already at much greater L-values (the electron is then effectively much more extended). Note, however, that this is not the only effect on the energy levels, another one is the fact that the electron-hole pair (exciton) may not be sufficiently separated leading to a band gap narrowing.[27–29]

Examples of trivial but very significant size effects are the decreased melting point of nano-crystalline metals,[30] the greatly enhanced F^--vacancy conduction in nano-crystalline CaF_2;[31] or the cross-over from ionic to electronic conductivity in CeO_2 as a function of grain size.[25,32] Whilst the CaF_2 experiment refers to accumulation layers, the CeO_2 experiment refers to the depletion layer situation already discussed above and will be considered in more detail now. Remember that a positive space charge potential (which we have found for polycrystalline CeO_2) implies the depletion of $V_O^{\bullet\bullet}$ and $h^\bullet$ while it leads to an accumulation of e'. If CeO_2 is sufficiently Gd_2O_3 doped such that [e′] in the bulk is small and $[V_O^{\bullet\bullet}]$ high, a dominant ionic conductivity is observed which is limited and determined by the depletion layers blocking the grain-to-grain transport ($\Delta\varphi = \sim 250$ mV). If the doping level is so small that a space charge potential of 250 mV is able to make the boundaries substantially *n*-conducting, indeed an unblocked electronic conductivity (along the parallel boundary paths) is observed. P_{O_2} and T dependencies measured for the serial depletion effect on the ions and the parallel accumulation effect on the electrons fit quantitatively together confirming the space charge model strongly.[23]

True size effects on ion conduction are observed in ionic superlattices composed of alternating epitaxial (111) CaF_2 and BaF_2 layers.[33] The thickness has been varied between 1 nm and 1 μm. The space charge effect can be quantitatively explained by a transfer of F^- from BaF_2 to CaF_2. Even at thicknesses below the Debye-length the conductivity still increases with decreasing spacing. In this regime the heterostructure is fully penetrated by overlapping space charge zones and an artificial ion conductor is generated (see Fig. 5).

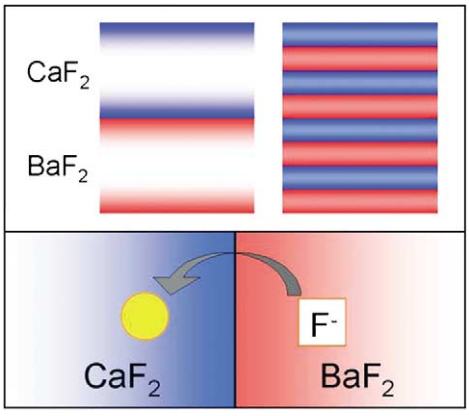

Fig. 5. Ionic heterostructures composed of CaF_2 and BaF_2 leading to mesoscopic ion conduction.[11]

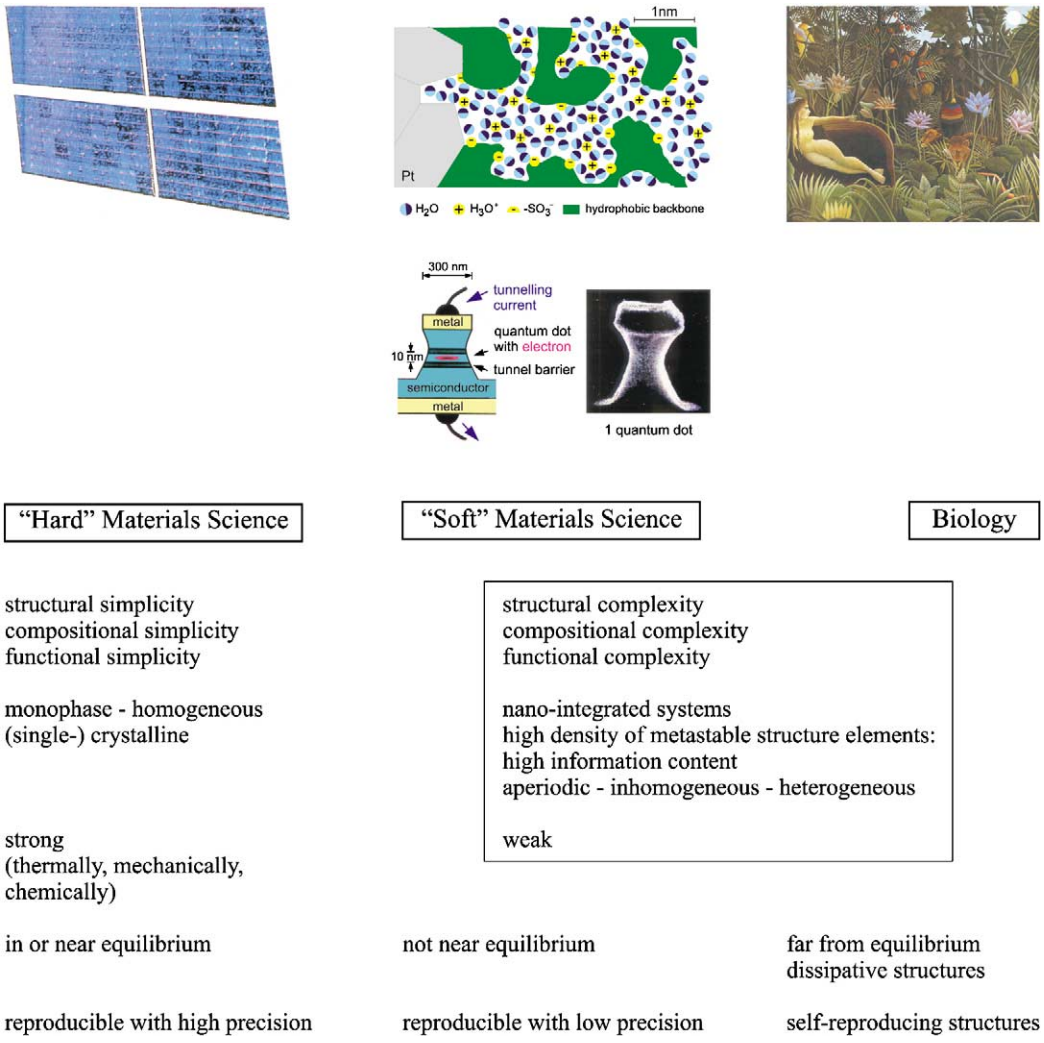

Fig. 6. The structuring on the nano-scale corresponds to a high density of metastable structure elements characterising a "soft materials science" with specific advantages and disadvantages: the figure gives a demarcation of "soft materials science" with respect to "hard" materials science and the other extreme case of biology, and stresses the common points with the latter (see box).[11] (Painting "The Dream" by Henri Rousseau, The Museum of Modern Art, New York.)

A nominally similar state is achieved in stacking fault structures observed in $AgI–Al_2O_3$, composites that can be conceived as heterolayers of γ-β-γ-β...AgI exhibiting superionic conduction.[34]

Already these few examples show the potential but also the complexity of "nano-ionics" which is even increased if ionic and electronic carriers which exhibit size-effects differently, are considered simultaneously and their mutual interaction is regarded. Many more phenomena have to be taken account of in a more precise consideration in a top-down approach: geometry effects, effects of capillary pressure, interactions between carriers, interaction of electrical field effects with structure, gradient effects, effects due to the discrete atomistic nature, phase transformations, and edge and corner energies. Bottom-up approaches starting from quantum-chemical cluster considerations are indispensable in order to obtain a full picture.

Irrespective of these difficulties nano-structuring allows the introduction of functional and structural complexity and variability in a similar way (see Fig. 6) as this is possible in organic chemistry (there on an atomistic level). It is worth noting that both situations rely on metastability: in the latter case on the metastability of the covalent molecules, in the former case on the morphological metastability owing to the metastability of higher-dimensional defects. Even though the morphology is surprisingly stable in the examples considered, applications for the field of electroceramics are restricted to low or moderate temperatures (see Fig. 4). Since, however, there is a general tendency to lower operational temperatures, nanostructured materials have a promising future as advanced electroceramics. Very recently reports on the benefit of nano-crystalline anodes and cathodes for Li-batteries testify this.[35]

References

1. Maier, J., Defect chemistry: composition, transport, and reactions in the solid state; part I: thermodynamics. *Angew. Chem., Int. Ed. Engl.*, 1993, **32**, 313–335.
2. Maier, J., *Festkörper—Fehler und Funktion: Prinzipien der Physikalischen Festkörperchemie*. B.G. Teubner Verlag, Stuttgart, 2000.
3. Denk, I., Münch, W. and Maier, J., Partial conductivities in $SrTiO_3$: bulk polarization experiments, oxygen concentration cell measurements, and defect-chemical modeling. *J. Am. Ceram. Soc.*, 1995, **78**, 3265–3272.
4. Kröger, F. A., Vink, H. J. and van den Boomgaard, J., Controlled conductivity in cadmium sulfide single crystals. *Z. Phys. Chem.*, 1954, **203**, 1–72; Smyth, D. M., Harmer, M. P. and Peng, P., Defect chemistry of relaxor ferroelectrics and the implications for dielectric degradation. *J. Am. Ceram. Soc.*, 1989, **72**, 2276–2278.
5. Waser, R. and Bulk conductivity, defect chemistry of acceptor-doped strontium titanate in the quenched state, *J. Am. Ceram. Soc.*, 1991, **74**, 1934–1940.
6. Sasaki, K. and Maier, J., Low-temperature defect chemistry of oxides. I. General aspects and numerical calculations. *J. Appl. Phys.*, 1999, **86**, 5422–5433; Sasaki, K. and Maier, J., Low-temperature defect chemistry of oxides. II. Analytical relations. *J. Appl. Phys.*, 1999, **86**, 5434–5443.
7. Maier, J., Ionic conduction in space charge regions. *Prog. Solid St. Chem.*, 1995, **23**, 171–263.
8. Maier, J., Point defect thermodynamics: macro- vs. nanocrystals. *Electrochemistry*, 2000, **68**, 395–402.
9. Jamnik, J., Maier, J. and Pejovnik, S., Interfaces in solid ionic conductors: equilibrium and small signal picture. *Solid State Ionics*, 1995, **75**, 51–58.
10. Maier, J., Defect chemistry conductivity effects in heterogeneous solid electrolytes. *J. Electrochem. Soc.*, 1987, **134**, 1524–1535.
11. Maier, J., Defect chemistry and ion transport in nano-structured materials (Aspects of nano-ionics. Part II). *Solid State Ionics*, 2003, **157**, 327–334.
12. Maier, J., On the conductivity of polycrystalline materials. *Ber. Bunsenges. Phys. Chem.*, 1986, **90**, 26–33.
13. Maier, J., Thermodynamic aspects and morphology of nano-structured ion conductors (Aspects of nano-ionics. Part I). *Solid State Ionics*, 2002, **154–155**, 291–301.
14. Holzinger, M., Fleig, J., Maier, J. and Sitte, W., Chemical sensors for acid-base-active gases: applications to CO_2 and NH_3. *Ber. Bunsenges. Phys. Chem.*, 1995, **99**, 1427–1432.
15. Fleig, J. and Maier, J., Microcontact impedance measurements of individual highly conductive grain boundaries: general aspects and application to AgCl. *Phys. Chem. Chem. Phys.*, 1999, **1**, 3315–3320.
16. Rodewald, S., Fleig, J. and Maier, J., Microcontact impedance spectroscopy at single grain boundaries in Fe-doped $SrTiO_3$ polycrystals. *J. Am. Ceram. Soc.*, 2001, **84**, 521–530.
17. Saito, Y. and Maier, J., Ionic conductivity enhancement of the fluoride conductor CaF_2 by grain boundary activation using Lewis acids. *J. Electrochem. Soc.*, 1995, **142**, 3078–3083.
18. Guo, X. and Maier, J., Grain boundary blocking effect in zirconia: a Schottky barrier analysis. *J. Electrochem. Soc.*, 2001, **148**, E121–E126.
19. Pike, G. E. and Seager, C. H., DC voltage dependence of semiconductor grain-boundary resistance. *J. Appl. Phys.*, 1979, **50**, 3414–3422.
20. Chiang, Y.-M. and Tagaki, T., Grain-boundary chemistry of barium-titanate and strontium-titanate. 1. High-temperature equilibrium space-charge. *J. Am. Ceram. Soc.*, 1990, **73**, 3278–3285.
21. Denk, I., Claus, J. and Maier, J., Electrochemical investigations of $SrTiO_3$ boundaries. *J. Electrochem. Soc.*, 1997, **144**, 3526–3536.
22. Leonhardt, M., Jamnik, J. and Maier, J., In situ monitoring and quantitative analysis of oxygen diffusion through Schottky-barriers in $SrTiO_3$ bicrystals. *Electrochem. Solid-State Lett.*, 1999, **2**, 333–335.
23. Kim, S. and Maier, J., On the conductivity mechanism of nanocrystalline ceria. *J. Electrochem. Soc.*, 2002, **149**, 373–383.
24. Guo, X., Sigle, W. and Maier, J., The blocking grain boundaries in yttria-doped and undoped ceria ceramics of high purity. *J. Am. Ceram. Soc.*, 2003, **86**, 77–87; Guo, X., Sigle, W., Fleig, J. and Maier, J., Role of space charge in the grain boundary blocking effect in doped zirconia. *Solid State Ionics*, 2002, **154–155**, 555–561.
25. Tschöpe, A., Grain size-dependent electrical conductivity of polycrystalline cerium oxide II: Space charge model. *Solid State Ionics*, 2001, **139**, 267–280.
26. Maier, J., Nano-sized mixed conductors (Aspects of nano-ionics. Part III). *Solid State Ionics*, 2002, **148**, 367–374.
27. Gräf, Ch.P., Heim, U. and Schwitzgebel, G., Potentiometrical investigations of nanocrystalline copper. *Solid State Ionics*, 2000, **131**, 165–174.
28. Rusanov, A. I., *Phasengleichgewichte und Grenzflächenerscheinungen*. Akademie-Verlag, Berlin, 1978.
29. Defay, R., Prigogine, I., Bellemans, A. and Everett, H., *Surface Tension and Adsorption*. John Wiley and Sons, New York, 1960.
30. Buffat, P. and Borel, J.-P., Size effect on melting temperature of gold particles. *Phys. Rev. A*, 1976, **13**, 2287–2298.
31. Puin, W., Rodewald, S., Ramlau, R., Heitjans, P. and Maier, J., Local and overall ionic conductivity in nanocrystalline CaF_2. *Solid State Ionics*, 2000, **131**, 159–164.
32. Tuller, H. L. and Nowick, A. S., Doped ceria as a solid oxide electrolyte. *J. Electrochem. Soc.*, 1975, **122**, 255–259.
33. Sata, N., Eberman, K., Eberl, K. and Maier, J., Mesoscopic fast ion conduction in nanometre-scale planar heterostructures. *Nature*, 2000, **408**, 946–949.
34. Lee, J.-S., Adams, S. and Maier, J., Transport and phase transition characteristics in $AgI:Al_2O_3$ composite electrolytes. Evidence for a highly conducting 7-layer AgI polytype. *J. Electrochem. Soc.*, 2000, **147**, 2407–2418.
35. Tarascon, J.-M. and Armand, M., Issues and challenges facing rechargeable lithium batteries. *Nature*, 2001, **414**, 359–367.